Structure of the Plasminogen Kringle 4 Binding Calcium-Free Form of the C-Type Lectin-Like Domain of Tetranectin

Steen Nielbo,[§] Jens K. Thomsen,[||] Jonas H. Graversen,[§] Peter Holme Jensen,[||] Michael Etzerodt,[§] Flemming M. Poulsen,*[,||] and Hans Christian Thøgersen[§]

Laboratory of Gene Expression, Department of Molecular and Structural Biology, University of Aarhus, Gustav Wieds Vej 10, DK-8000 Aarhus C, Denmark, and SBIN Lab, Department of Protein Chemistry, Institute of Molecular Biology, University of Copenhagen, Øster Farimagsgade 2A, DK-1353 Copenhagen, Denmark

Received March 3, 2004; Revised Manuscript Received May 10, 2004

ABSTRACT: Tetranectin is a homotrimeric protein containing a C-type lectin-like domain. This domain (TN3) can bind calcium, but in the absence of calcium, the domain binds a number of kringle-type protein ligands. Two of the calcium-coordinating residues are also critical for binding plasminogen kringle 4 (K4). The structure of the calcium free-form of TN3 (apoTN3) has been determined by NMR. Compared to the structure of the calcium-bound form of TN3 (holoTN3), the core region of secondary structural elements is conserved, while large displacements occur in the loops involved in calcium or K4 binding. A conserved proline, which was found to be in the cis conformation in holoTN3, is in apoTN3 predominantly in the trans conformation. Backbone dynamics indicate that, in apoTN3 especially, two of the three calcium-binding loops and two of the three K4-binding residues exhibit increased flexibility, whereas no such flexibility is observed in holoTN3. In the 20 best nuclear magnetic resonance structures of apoTN3, the residues critical for K4 binding span a large conformational space. Together with the relaxation data, this indicates that the K4-ligand-binding site in apoTN3 is not preformed.

Tetranectin (TN),[1] a protein found in human (*1*) and several animal species, is expressed by many different cell types and is present in human serum at a concentration of 10 mg/L (*2*). Roles for TN have been reported in several types of cancer, where a higher level of TN in the blood is correlated with higher survival rates (*3*). In addition, TN has been shown to accumulate in the stroma of breast, ovarian (*4*), and colon (*5*) carcinomas and to colocalize with plasminogen at the invasive front of melanomas (*6*). Roles for TN have also been reported in myogenesis (*7*) and bone development (*8*, *9*), and mice with a deletion of the TN gene exhibit a spinal deformity (*10*). These implications in development and diseases indicate a role for TN in processes involving tissue remodeling.

TN is a homotrimeric protein (*11*). An N-terminal short lysine-rich region binds complex-sulfated carbohydrates including heparin (*12*). This region is followed by an α-helix domain, responsible for the trimerisation (*13*, *14*) of TN, and a C-terminal C-type lectin-like domain (CTLD), which is encoded by the third exon of the TN gene and therefore is called TN3.

TN3 can bind two calcium ions, such as many other CTLDs, but in the absence of calcium, TN3 can bind to the kringle 4 domain of plasminogen (Plg K4). The interaction between plasminogen and TN has been reported to facilitate the proteolytic activation of plasminogen to plasmin (*1*). In TN3, two of the residues involved in the coordination of calcium are also critical for the binding of K4 (*15*). In Plg K4, three residues in the lysine-binding pocket and at least one residue not involved in lysine binding are critical for the interaction with TN3 (*16*). In addition to plasminogen, the kringle proteins apolipoprotein(a) (*17*, *18*), hepatocyte growth factor, and tissue-type plasminogen activator (*19*) have also been reported to bind to TN. For the latter two, the interaction with TN has not been mapped in detail and sensitivity to inhibition by calcium was not reported; however, it must be assumed that binding is taking place through TN3.

CTLDs are common modules found in extracellular animal proteins and are defined by sequential and structural homology to the subgroup defining the prototype, the carbohydrate recognition domains (CRDs) of animal C-type lectins. The broader term CTLD is being used to comprise domains binding a variety of other ligands than just carbohydrates, including proteins and inorganic surfaces of ice or $CaCO_3$

† We thank The John and Birthe Meyer Foundation for the donation to establish the SBIN Lab.

‡ Protein Data Bank entry: 1RJH.

* To whom correspondence should be addressed: SBIN Lab, Department of Protein Chemistry, Institute of Molecular Biology, University of Copenhagen, Øster Farimagsgade 2A, DK-1353 Copenhagen, Denmark. E-mail: fmp@apk.molbio.ku.dk. Phone: +45-3532-2077. Fax: +45-3532-2075.

§ University of Aarhus.

|| University of Copenhagen.

[1] Abbreviations: ApoTN3, calcium-free form of TN3; CTLD, C-type lectin-like domain; HoloTN3, TN3 with two calcium ions bound; HSQC, heteronuclear single-quantum coherence; K4, plasminogen kringle domain number 4; MBP, mannose-binding protein; MMR−CRD4, CRD4 of macrophage mannose receptor; NMR, nuclear magnetic resonance; NOE, nuclear Overhauser effect; RMSD, root-mean-square deviation; TN, tetranectin (residues 1−181); TN3, residues 45−181 of full-length TN, corresponding to the CTLD and 5 additional residues.

10.1021/bi049570s CCC: $27.50
Published on Web 06/18/2004

(*20*). The general CTLD motif consists of a core of conserved secondary structural elements and a loop region, often binding calcium, where the most significant structural differences among CTLDs are found. The carbohydrate binding of CTLDs is located in the loop region, and several CTLDs, including TN3, bind other types of ligands to the same region. So far, TN3 represents the only example of a CTLD that is able to bind calcium but, in the absence of calcium, has the affinity to bind protein ligands. Understanding the conformational changes governing the binding of calcium or K4 by TN3 may therefore provide new insight into relationships between structure and function of CTLDs.

A crystal structure of TN at 2.8 Å resolution (*13*) and a crystal structure of TN3 at 2.0 Å (*21*) have previously been reported. Both structures correspond to the holo form of TN with two calcium ions bound by the CTLD. To gain further insight into the interaction between TN and plasminogen, the present structure addresses the structure and dynamics of the calcium-free, K4-binding form of TN3.

MATERIALS AND METHODS

The rTN3 expression vector and the protocol for expression, refolding, and purification have been described earlier (*11*). Uniformly $^{13}C/^{15}N$-labeled protein was produced by growing *Escherichia coli* BL21DE3pLys cells in M9 minimal medium with $(^{15}NH_4)_2SO_4$ and $[^{13}C_6]$-glucose as the sole sources for nitrogen and carbon. A protein concentration of 0.6 mM in 90% H_2O/10% D_2O containing 1 mM NaN_3 at pH 6.7 was obtained using the Centricon YM-10 concentrating device (Millipore). The holoTN3 sample was prepared by adding $CaCl_2$ to a final concentration of 2 mM.

The NMR data were acquired at 298 K on a Varian Unity Inova 800 MHz instrument. Nearly complete backbone and side-chain assignments were obtained using the following standard experiments from the Varian Proteinpack: ^{15}N-HSQC, HNCO, HN(CA)CO, HNCA, HN(CO)CA, HNCACB, CBCA(CO)NH, ^{15}N-edited TOCSY−HSQC, HCCH−TOCSY, ^{15}N-edited NOESY−HSQC, and ^{13}C-edited NOESY−HSQC.

Relaxation data (T_1 and T_2) and heteronuclear $\{^1H\}$-^{15}N NOEs were acquired at 298 K on a Varian Unity Inova 750 MHz instrument. T_1 and T_2 values were determined from a nonlinear least-squares fit to an exponential curve of measured peak heights as a function of the delay. The $\{^1H\}$-^{15}N NOE saturation values were determined as the I_{sat}/I_{unsat} ratio from two spectra recorded with and without proton saturation. All spectra were processed with NMRpipe (*22*) and analyzed with PRONTO (*23*). Resonance signals from the peptide backbone atoms were assigned with the aid of AUTOASSIGN (*24*).

The residue numbering used corresponds to the numbering of full-length TN. The secondary structure and loop topology found in the crystal structure of holoTN3 (1TN3) has been used as a reference. The core region of TN3 refers to residues 69−114 and 154−179, which contain the secondary structural elements. All molecular graphic presentations were prepared using Molmol (*25*).

RESULTS

^{15}N-HSQCs of Apo- and HoloTN3. A superposition of ^{15}N-HSQCs of apo- and holoTN3 indicates that major conformational differences exist between the two forms, because many nonoverlapping peaks can be observed (Figure 1). For holoTN3, the peaks are sharper than for apoTN3 and a slightly broader dispersion can be observed, indicating that the overall structure of holoTN3 is better defined as compared to that of apoTN3. In two differential scanning calorimetry experiments, the melting temperature was measured to 57 °C for apoTN3 and 68 °C for holoTN3 (data not shown). This demonstrates the stabilizing effect of the binding of calcium ions to TN3.

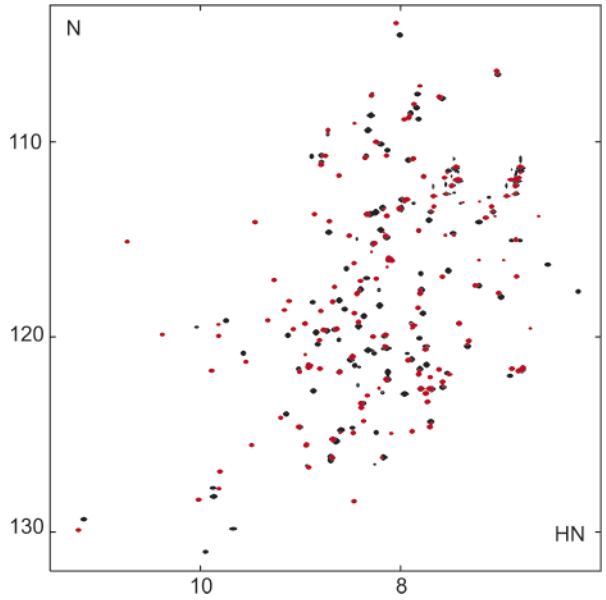

FIGURE 1: ^{15}N-HSQC of apo- and holoTN3. Black = apoTN3 and red = holoTN3. The many nonoverlapping peaks indicate major structural differences between apo- and holoTN3. The broader dispersion of holoTN3 and the slightly broader line width of apoTN3 indicate that the structure of holoTN3 is less dynamic than the structure of apoTN3.

Backbone and Side-Chain Assignments in ApoTN3. The TN3 construct corresponds to residues 45−181 of full-length TN. This comprises the CTLD (50−181) and five additional residues in the N terminal. For residues 64−181, nearly complete sequence-specific backbone and side-chain assignments could be obtained using ^{13}C-/^{15}N-labeled protein and standard triple-resonance experiments. For the residues Asn93, Thr122, Val124, Asn135, Ile180, and Val181, no NMR signals could be assigned for the backbone atoms. For residues 151−153, located at the end of loop 4, neither backbone nor side-chain resonances could be assigned. For all assigned residues, sequential backbone correlations and/or sequential NOEs could be observed.

Side-chain assignments were obtained from ^{15}N-TOCSY−HSQC and ^{13}C-HCCH−TOCSY experiments. Aromatic rings, amide groups, and methionine methyl groups were assigned through NOEs from ^{15}N-NOESY−HSQC and ^{13}C-NOESY−HSQC experiments. Among the sequentially assigned residues, side-chain assignments for nonlabile protons are complete with the following exceptions: Thr86$^{H\beta,H\gamma2}$, Leu96$^{H\gamma}$, Trp136$^{H\delta1,H\epsilon3}$, Trp163$^{H\delta1}$, Arg167$^{H\epsilon}$, and Arg169$^{H\epsilon}$. Amide groups could be assigned for Gln88, Gln102, Asn106, Asn160, and Gln171.

Indications of Disorder in the N Terminal of TN3. For residues 45−63, no NMR signals were observed, indicating line broadening from slow conformational exchange of the

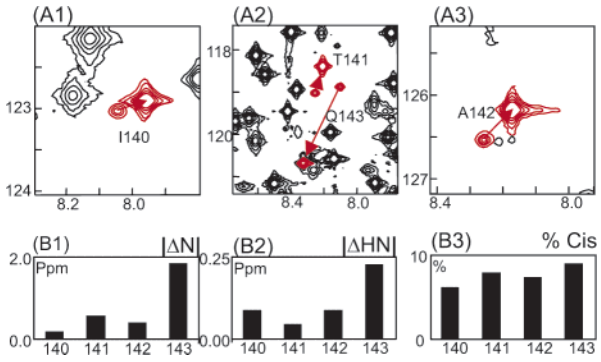

FIGURE 2: Evidence for two conformations at Pro144. (A1−A3) Regions in the ^{15}N-HSQC of apoTN3 where two resonances for the residues I140, T141, A142, and Q143 (colored in red) are observed. The minor conformation corresponds to the cis conformation. (B1 and B2) Differences in ^{15}N and HN chemical shifts between the two peaks assigned to each of the 4 residues. (B3) Intensities of the weak peaks relative to the strong peaks.

N-terminal part of the recombinant construct. A backbone assignment of holoTN3 confirmed this observation, indicating that the disorder of the N terminal is not related to the presence or absence of calcium. This part of the construct is not represented in the final structure.

In the structure of full-length TN, the helix involved in the trimerisation (E2) proceeds to residue 52 followed by a short β strand (B0 = residues 53−56), a turn, and another β strand (B1 = residues 59−65) (*13*). The N-terminal residues that could not be assigned in apo- or holoTN3 are in the crystal structure of holoTN3 involved in the formation of two of the three strands in a β sheet (B0′ = 45−52, B1 = 58−65, and B5 = 174−179), which packs against the same sheet from a crystallographically related monomer (*21*). Thus, the residues that could not be assigned by NMR adopt different conformations in the crystal structures of full-length TN and holoTN3. This may suggest that the N-terminal β-sheet structure in the X-ray structure of holoTN3 is a result of the crystal-lattice packing, while it is not a major conformation in solution. Because the overall structure of apoTN3 still closely matches the crystal structure of holoTN3, the residues 45−64 are not critical for the folding of the domain. This is further supported by the fact that mutations of Cys50 and Cys60 to prevent formation of the N-terminal disulfide bridge did not affect the overall stability of the CTLD (unpublished results).

Evidence for Two Conformations of Pro144 in ApoTN3. In all structures of CTLDs with calcium bound, including the crystal structures of holoTN and holoTN3, the peptide bond preceding a conserved proline (Pro144 in TN) adopts the cis conformation. In the backbone spectra of apoTN3, two NMR signals were observed for each of the four residues preceding Pro144 (Figure 2). This is interpreted as evidence that Pro144 can adopt both the cis and trans conformation. For each of the residues 140−143, the ratio between the intensities of the two peaks indicates approximately 90% of the major conformation. Only this major conformation can be observed in the less sensitive side-chain spectra. For Pro87, Pro173, and the major conformation of Pro144, strong $d_{\alpha\delta}$ or $d_{\beta\delta}$ NOE connectivities between the prolines and the subsequent residues are evidence of the trans conformation (*26*). We therefore conclude that the peptide bond preceding Pro144 in apoTN3 is in the trans conformation in 90% of the molecules.

Comparison of Chemical Shifts in Apo- and HoloTN3. To investigate differences in structural and dynamic properties between apo- and holoTN3, a backbone assignment of holoTN3 was performed. The assignment of holoTN3 generally confirms the assignment of apoTN3. As for apoTN3, the N-terminal 20 residues could not be assigned in holoTN3, and for those residues that have been assigned in both forms, only minor chemical-shift differences occur in large parts of the protein. The largest chemical-shift differences are located in three intervals corresponding to L1, from L3 through L4 into B3, and the end of B4. The intervals with the larger chemical-shift changes closely match the location of the calcium-binding residues (Figure 3), and if mapped on the structure of holoTN3, they form a contiguous region around the calcium ions (Figure 4). This indicates that the core secondary structure of apoTN3 is the same as in holoTN3 and that the major structural changes are restricted to the loop regions.

NOE Assignment and Structure Calculations. For apoTN3, a complete structure determination was performed. Using the software Pronto (*23*), 9147 peaks from ^{15}N-NOESY−HSQC and ^{13}C-NOESY−HSQC spectra were interactively picked. The chemical-shift list, the unassigned peak lists, and the peak heights were used as input for CYANA (*27*, *28*), which includes the CANDID protocol for automatic NOE assignment and structure calculation. As additional input, upper-distance limits for the disulfide bonds Cys77−Cys176 and Cys152−Cys168, the coordinates from the crystal structure of holoTN3 as the start structure, and initially 231 dihedral-angle constraints from TALOS (*29*) with a tolerance of ±30° were used. This yielded 1910 nonredundant upper-limit constraints as output from CYANA, with 156 upper-limit constraints being violated with more than 0.5 Å and 110 dihedral-angle constraints being violated with more than 5°. In all of the structures calculated in this first stage, the overall fold was the same. The secondary structure elements were very similar to those found in the crystal structure of holoTN3, whereas the loop regions were poorly defined.

The violated constraints were refined through iterative rounds of structure calculations with the CYANA protocol ANNEAL. When all violated constraints were increased to 5.5 Å, approximately 90% of the violations were eliminated and subsequently the remaining violations were evaluated by inspection. Violated angle constraints were used with increased tolerance (±10°) or removed if they continued to be violated. The overall fold was not affected by the refinement of the constraint dataset, but the root-mean-square deviation (RMSD) was slightly increased for the secondary structure elements and more significantly increased in the loop regions.

The lowest energy structure and the NOE and dihedral-angle constraint datasets obtained from CYANA were used for the calculation of 200 structures with XPLOR-NIH version 2.9.1 (*30*), using a simulated annealing protocol. The 20 lowest energy structures were refined with CNS version 1.1 (*31*), using a simulated annealing protocol with an explicit layer of water (*32*). The use of first XPLOR-NIH and then CNS did not affect the overall structure, but in each case, it did improve the Ramachandran plot distribution and decrease the RMSD relative to the crystal structure of holoTN3.

The final structures have no NOE violations above 0.4 Å and no angle violations above 5°. An overview of the results

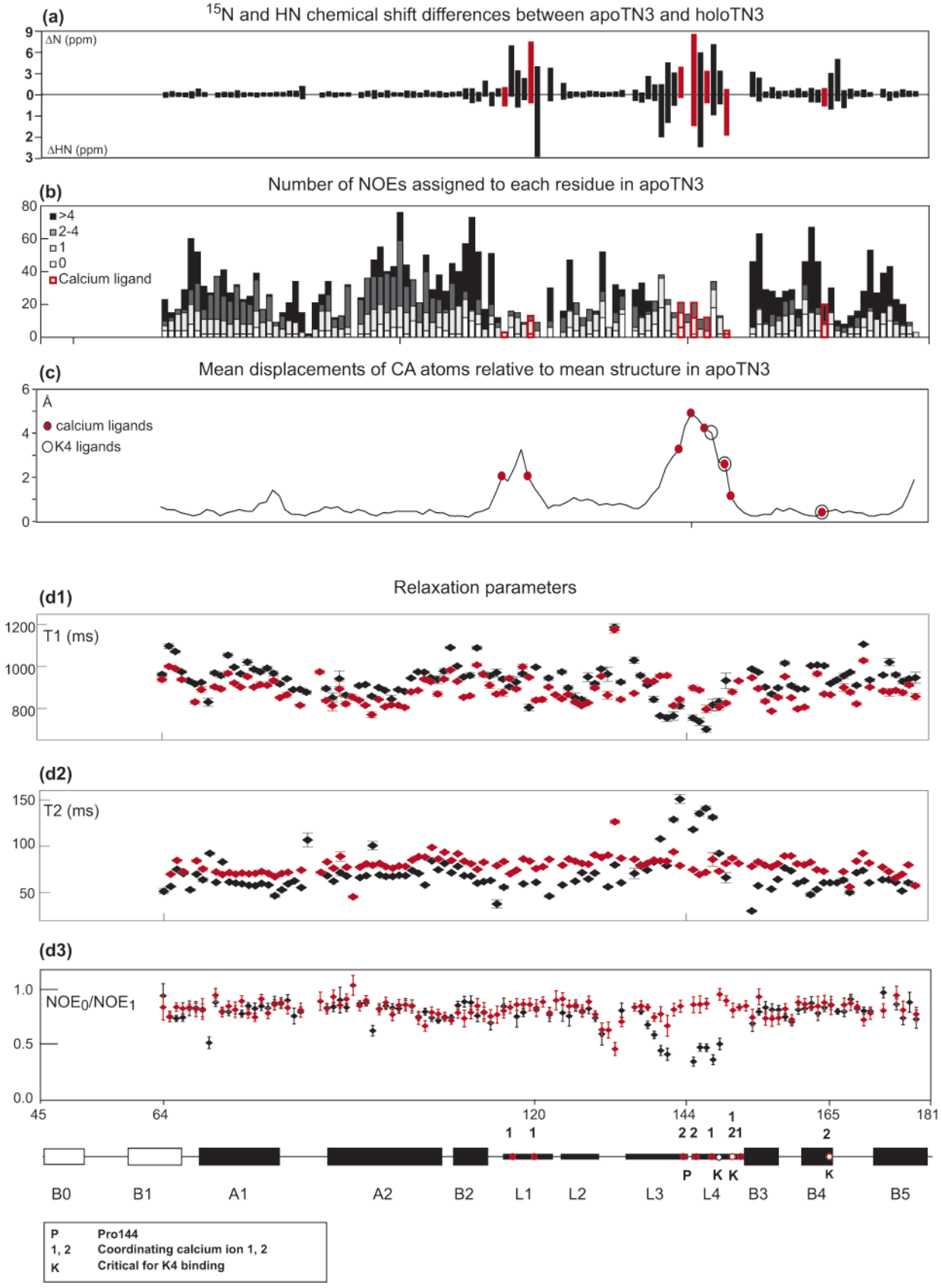

FIGURE 3: Sequential data plots. (a) Chemical-shift differences between apo- and holoTN3. Absolute differences are shown for ^{15}N (above the axis) and HN (below the axis). Calcium-coordinating residues are highlighted in red. (b) Number of NOEs assigned to each residue, grouped into intra (0, white), sequential (1, light gray), medium (2−4, dark gray), and long range (>4, black). The calcium-coordinating residues have red borders. (c) Displacements of CA atoms relative to the mean structure in apoTN3. Calcium-coordinating residues are highlighted in red and K4-binding residues are indicated with black circles. (d1−d3) T1, T2, and NOE values, respectively. (Bottom) The secondary structure topology as observed in the crystal structure of holoTN3. B0 and B1, shown as white boxes, have not been assigned in apoTN3.

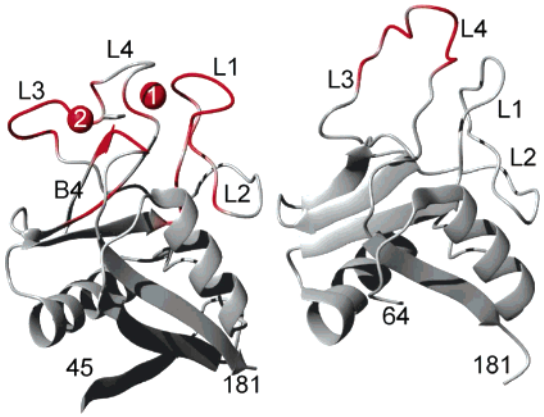

FIGURE 4: Regions with most affected chemical shifts and relaxation parameters. (Left) Residues with the largest ^{15}N and HN chemical-shift differences between apo- and holoTN3 have been mapped on the crystal structure of holoTN3 (1TN3). The most affected region closely matches the location of the calcium ions. (Right) Most dynamic residues in apoTN3 have been mapped on the lowest energy NMR structure of apoTN3. Increased flexibility is observed in L3 and L4, which are both involved in calcium binding. For L1, which is also involved in calcium binding, no increase in the dynamics is observed.

Table 1: Structural Statistics for ApoTN3[a]

distance restraints	1552
intraresidual	195
sequential (1)	439
medium range (2−4)	386
long range (>4)	532
dihedral-angle restraints	194
Φ	98
Ψ	96
NOE distance-constraint violations	
number > 0.3 Å	1
maximum (Å)	0.39
dihedral angle violations	
number > 5°	0
CNS water-refinement energies[b]	
overall	−4835 ± 124
bonds	28 ± 2
angles	144 ± 13
impropers	90 ± 5
dihedral angles	670 ± 9
van der Waals	−500 ±17
electric	−5292 ± 106
NOE restraints	22 ± 6
dihedral-angle restraints	3 ± 2
RMSD relative to the mean (Å)[b]	
backbone atoms, core[c]	0.58 ± 0.09
heavy atoms, core[c]	1.06 ± 0.12
backbone atoms, all	1.31 ± 0.27
heavy atoms, all	1.69 ± 0.23
Ramachandran values	
most favored regions (%)	85.2
additionally allowed regions (%)	12.8
generously allowed regions (%)	1.8
disallowed regions (%)	0.2

[a] Energies were calculated with CNS version 1.129, using a simulated annealing protocol with an explicit layer of water (*30*). [b] kcal/mol, average ± standard deviation. [c] Residues 69−114 and 154−179.

for the 20 best structures is given in Table 1, and the structure is shown in Figure 5.

The number of NOEs assigned to each residue is shown in Figure 3. It illustrates that the number of long-range constraints as well as the total number of constraints are lowest in the loop regions. This is also reflected in the higher RMSD values for the residues in these regions (Figure 3).

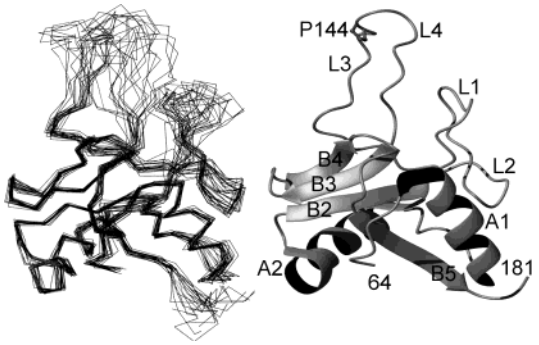

FIGURE 5: NMR structure of apoTN3. (Left) CA trace of the 20 lowest energy structures. The core regions (residues 64−114 and 154−179) have been aligned using Molmol (*25*). (Right) Ribbon representation of the lowest energy structure with Pro144 shown. The poor definition of the loops L3 and L4 is in agreement with the increased flexibility indicated by the relaxation parameters for this region.

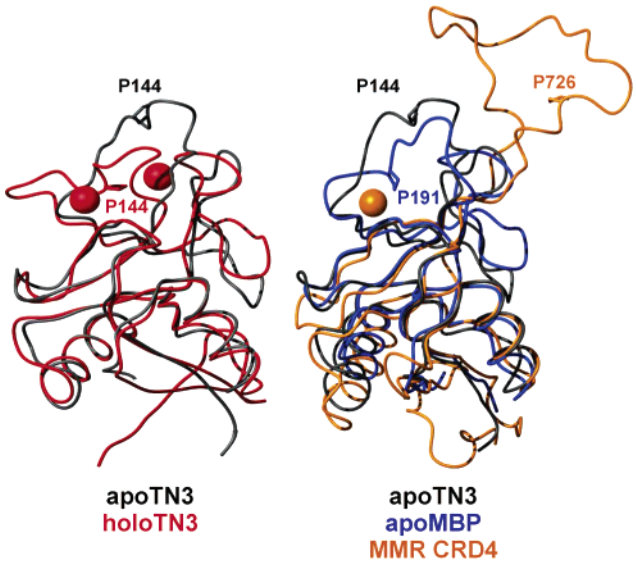

FIGURE 6: Structural alignments. (Left) apoTN3 (grey) and holoTN3 (1TN3, red). (Right) apoTN3 (grey), apoMBP (1BV4, blue), and MMR−CRD4 (1EGI, orange). The conserved prolines in the calcium-binding sites are also shown. The structures were aligned with SwissPdbViewer (*40*). In apo- and holoTN3, the core structure is conserved, whereas large conformational changes occur in the loops. The structures of apoTN3, apoMBP, and MMR−CRD4 illustrate different levels of disorder in the loop regions in the partial or complete absence of calcium. In the structure of MMR−CRD4, a calcium ion is found in the canonical calcium-binding site 2 only, although the molecule is known to bind two calcium ions.

Structural Comparison with HoloTN3. A structural alignment of the NMR structure of apoTN3 and the crystal structure of holoTN3 confirms that the core secondary structure of TN3 is essentially the same in the apo and holo forms. For the residues defining the core structure, the backbone atoms of the lowest energy NMR structure of apoTN3 (NMR) and the crystal structure of holoTN3 (X-ray) align with a RMSD of 0.60 Å (Figure 6).

In contrast to the core region, major structural differences occur in the loop regions. The most striking difference is that the residues corresponding to L3 and L4 in holoTN3 form one loop in apoTN3. However, because of the lack of long-range NOE constraints in this region (Figure 3b), the conformations of the loops are not well-determined (Figure 5). The calcium-ligating residues are Asp116, Glu120,

Glu143, Asp145, Gly147, Glu150, Asn151, and Aspl65 (*21*), and the residues critical for K4 binding are Lys148, Glu150, and Asp165 (*15*). Except for Asp165, all of these residues are located in the loops, and as a consequence, their positions are poorly defined.

Backbone Dynamics of Apo- and HoloTN3. To further characterize different properties of apo- and holoTN3, backbone dynamics were analyzed by measuring longitudinal (T1) and transverse (T2) relaxation rates and {^{1}H}-^{15}N-heteronuclear NOEs. The results are summarized in Figure 3.

The results indicate similar relaxation rates for apo- and holoTN3 for the major part of the residues. However, a tendency for longer T_1 values and shorter T_2 values can be observed for apoTN3, indicating a longer correlation time. Using the Liparo−Szabo model-free formalism, the overall tumbling time could be estimated to 9.5 ns for apoTN3 and 8.2 ns for holoTN3. This correlates well with the fact that apoTN3 is less compact because of the extended-loop region.

For the fragment consisting of residues 139−149, which corresponds to L3−L4 in holoTN3, significantly lower NOE values, higher T_2 values, and lower T_1 values are observed for apoTN3, whereas holoTN3 has values comparable to the rest of the protein in this region. L3 and L4 harbor three of the six calcium-coordinating residues, and the results indicate that in the absence of calcium the backbone atoms in this region exhibit increased flexibility on a pico- to nanosecond time scale. This may be of significant importance for the biological function of TN, because two of the three residues, which are critical for plasminogen binding (Lys148 and Glu150), are located in loop 4.

In the segments corresponding to L1−L2 and B3−B4, T_2 values appear to be very short in apoTN3. The remaining three residues involved in calcium coordination (Asn115 and Glu120 in L1 and Asp165 at the end of B4) are located in these segments, and the observations suggest exchange processes on a slower time scale than the one found in the L3−L4 region.

Thus, in apoTN3, two of the calcium-binding loops (L3 and L4) exhibit flexibility on a fast time scale, whereas L1 and the end of B4, which also are involved in calcium binding may be involved in intermediate-exchange processes. Together, the large RMSD values and the backbone dynamics both indicate that, in the NMR structure of apoTN3, neither the calcium-binding site nor the K4-binding site is well-defined.

DISCUSSION

CTLD Loop Regions. The conserved core structure and the dramatic structural changes in the loops of apoTN3 are in agreement with the crystal structures of the CTLDs of mannose-binding protein (MBP) with and without calcium bound (*33*). In the crystal structure of apoMBP, four conformations of the loop region are found in the asymmetric unit, most likely representing different conformations in solution. This agrees well with the large conformational space spanned by L3−L4 in the 20 best NMR structures of apoTN3. However, in all four copies of apoMBP, the residues corresponding to L3−L4 still form two distinct loops, in contrast to the one extended loop (L34) in apoTN3 (Figure 6).

The residues corresponding to L3−L4 in apoTN3 forming one big loop are similar to the structure of CRD4 in the macrophage mannose receptor (MMR−CRD4), in which calcium was only bound to the canonical calcium site 2. The residues corresponding to L1−L4 form a large loop (Figure 6), which by domain swapping packs against the secondary structure core of a symmetry-related molecule (*34*). MMR−CRD4 is capable of binding two calcium ions (*35*). Although no structure of MMR−CRD4 with two calcium ions and a compact-loop region has been reported, it is believed to exist for MMR−CRD4 to bind its carbohydrate ligands. The crystal structure with the extended-loop conformation is thought to represent a partly unfolded endosomal form.

MBP, TN3, and MMR−CRD4, which are all able to bind two calcium ions in the loop region, thus exhibit three levels of structural disorder in the absence of one or two of the calcium ions. In all three cases, the structures indicate that the loops in the absence of calcium are flexible. However, in MBP, four distinct loops can still be observed in the apo form; in apoTN3, residues corresponding to L3−L4 form one loop; and in MMR−CRD4, residues corresponding to L1−L4 form a single extended loop, when the calcium ion in site 1 is lost (Figure 6). The structure of apoTN3 is thus further evidence that CTLDs consist of conserved core structures with loop regions that are able to adopt a variety of conformations.

Cis−Trans Isomerization of Pro144. Pro144 in TN3, which is conserved in many CTLDs, adopts the cis conformation in all known structures of CTLDs with calcium bound. In the solution structure of apoTN3, this proline adopts the trans conformation and there is evidence for a minor fraction of approximately 10% of the molecules displaying a different conformation, interpreted as the cis conformation. This is in agreement with results for apoMBP, where both the cis and trans conformation of the corresponding proline are found in the same crystal (*33*), and fluorescence experiments indicate that in apoMBP approximately 80% of these prolines adopt the trans conformation (*36*). In apoTC14, missing signals for the two residues following Pro87 are suggested to result from conformational flexibility in this region (*37*). Although there is no proof for cis−trans isomerization of Pro87 in apoTC14, this increased flexibility could corroborate the assumption that Pro87 is able to adopt more than one conformation

Dynamics of CTLD Ligand-Binding Loops. The increased flexibility in the calcium-binding loops of apoTN3 is evidence for the stabilization of the structure upon calcium binding as is often observed upon ligand binding. The result is, however, in contrast to results reported for the C-type lectin TC14, where the dynamics of the ligand-binding loops are the same as those for the rest of the protein both with and without calcium bound (*37*). TC14 binds D-galactose, and it is suggested that the conformational stability of the ligand-binding region may be a prerequisite for the precise positioning of the ligand-binding residues to bind a small ligand with high specificity. For apoTN3, the flexibility may reflect that the conformation of a protein ligand is less strictly defined than the conformation of a carbohydrate ligand.

In addition to the conserved proline bridging loop 3 and loop 4 (Pro87 in TC14 and Pro144 in TN3), TC14 contains three additional proline residues in loop 2 and 3, which may contribute to the rigidity of the loops. These residues are

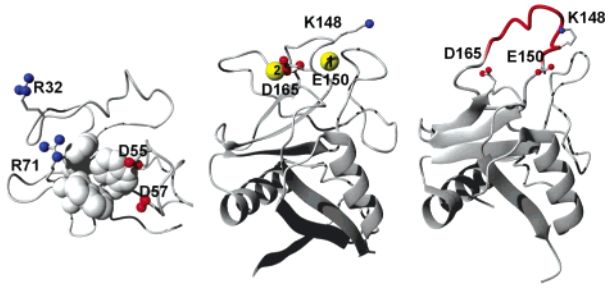

FIGURE 7: Interacting residues in K4 and TN3. (Left) K4 (1PK4). (Center) holoTN3 (1TN3). (Right) The lowest energy NMR structure of apoTN3 (1RJH). The critical charged residues are shown as ball and stick models, and the calcium ions (1 and 2) in holoTN3 are shown as yellow spheres. On apoTN, the most dynamic part of the backbone is colored in red. With respect to the K4-binding residues in TN3, two major differences between apo- and holoTN3 should be noted: In holoTN3, the two negatively charged residues are close in space, because they are coordinating the same calcium ion, and their charges are counteracted by the calcium ion. In apoTN3, residues K148 and E150 are exposed and located in a flexible region of the protein. Thus, in apoTN3, the binding site seems able to adopt a conformation suitable for K4 binding, whereas this is clearly not the case in holoTN3.

not found in TN3 and may be one reason for the conformational stability of the loops in apoTC14.

The reduced dispersion and slightly increased line width in the ^{15}N-HSQC of apoTN3 relative to holoTN3 also indicates that the structure of apoTN3 is less well-defined because of the absence of calcium. Also this is in contrast to the results found for TC14, where the holo form yields broader lines than the apo form. For TC14, two factors may reverse the observed pattern relative to TN3. One factor is that because the loops also in TC14 are less dynamic they cannot contribute to line broadening of the apo form relative to the holo form as is the case for apoTN3. In addition, the major dimeric form of holoTC14 is in equilibrium with approximately 5% of higher order aggregates (*38*), and it has been suggested that this aggregation is mediated by the presence of calcium (*37*). This would contribute to a higher average molecular weight, slower tumbling, and hence broader line width of holoTC14 relative to apoTC14. Both apo- and holoTN3 are monomers in solution and are therefore not subject to the same line-broadening effects from dimerization or multimerization.

Interaction between Plg K4 and TN3. The binding of lysine analogues to K4 depends on the positively charged residue Arg71 and on the negatively charged residues Asp55 and Asp57. In addition, Arg32 is also important for the binding to TN3. Similarly, in apoTN3, the positively charged residue Lys148 and the two negatively charged residues Glu150 and Asp165 are important for binding to K4. In holoTN3, Glu150 and Asp165 are involved in calcium-ion binding. Clearly, the removal of the calcium ions from TN3 exposes the two negatively charged residues and makes these available for polar interactions with either or both of the positively charged residues Arg32 and Arg71 on K4. The release of the calcium ions from TN3 also increases the pico- to nanosecond backbone dynamics at Glu150 and Lys148, whereas the backbone dynamics at Asp165 indicate an exchange process on a slower time scale. This suggests that together the three residues, Lys148, Glu150, and Asp165, may be able to adopt a conformation that may permit optimal polar interactions with the counterions on Plg K4 (Figure 7).

Extracellular Calcium Switch. The ability of calcium to inhibit the interaction between TN and plasminogen may provide a means of regulation. The dissociation constants for the interaction between TN3 and the two calcium ions are 37 and 61 μM (unpublished results), whereas K_d for the interaction between TN3 and K4 is 50 μM (*15*). The concentration of free Ca^{2+} in the blood is normally tightly controlled at a concentration of 1 mM, which is enough to keep TN in the calcium-saturated state. However, the role of calcium ions as extracellular messengers is becoming well-established, and increasing numbers of mechanisms regulated by local changes of the extracellular calcium levels have been reported (*39*). An interaction between TN and plasminogen mediated by a local decrease in the calcium concentration therefore seems plausible, and it can be speculated that one or more other calcium-binding proteins must be involved in the regulation of the calcium-saturation state of TN and thereby play a role in the biological mechanism of the interaction between TN and plasminogen.

ACKNOWLEDGMENT

We thank associate professor Bent Sigurskjold (August Krogh Institute, University of Copenhagen) for recording differential scanning calorimetry experiments and lab technicians Ove Lillelund and Anette Kjems for excellent technical assistance in protein production.

SUPPORTING INFORMATION AVAILABLE

Chemical shifts for apoTN3 (entry 6007) and holoTN3 (entry 6008) deposited in the BioMagResBank. This material is available free of charge via the Internet at http://pubs.acs.org.

REFERENCES

1. Clemmensen, I., Petersen, L. C., and Kluft, C. (1986) Purification and characterization of a novel, oligomeric, plasminogen kringle 4 binding protein from human plasma: Tetranectin, *Eur. J. Biochem. 156*, 327−333.
2. Jensen, B. A., McNair, P., Hyldstrup, L., and Clemmensen, I. (1987) Plasma tetranectin in healthy male and female individuals, measured by enzyme-linked immunosorbent assay, *J. Lab. Clin. Med. 110*, 612−617.
3. Høgdall, C. K. (1998) Human tetranectin: Methodological and clinical studies, *APMIS Suppl. 86*, 1−31.
4. Høgdall, C. K., Christensen, L., and Clemmensen, I. (1994) Tetranectin, a plasma and tissue protein—a prognostic marker of breast and ovarian cancer, *Ugeskr. Laeg. 156*, 6190−6195.
5. Wewer, U. M., and Albrechtsen, R. (1992) Tetranectin, a plasminogen kringle 4-binding protein. Cloning and gene expression pattern in human colon cancer, *Lab. Invest. 67*, 253−262.
6. De Vries, T. J., De Wit, P. E., Clemmensen, I., Verspaget, H. W., Weidle, U. H., Bröcker, E. B., Ruiter, D. J., and Van Muijen, G. N. (1996) Tetranectin and plasmin/plasminogen are similarly distributed at the invasive front of cutaneous melanoma lesions, *J. Pathol. 179*, 260−265.
7. Wewer, U. M., Iba, K., Durkin, M. E., Nielsen, F. C., Loechel, F., Gilpin, B. J., Kuang, W., Engvall, E., and Albrechtsen, R. (1998) Tetranectin is a novel marker for myogenesis during embryonic development, muscle regeneration, and muscle cell differentiation in vitro, *Dev. Biol. 200*, 247−259.
8. Iba, K., Sawada, N., Chiba, H., Wewer, U. M., Ishii, S., and Mori, M. (1995) Transforming growth factor-b1 downregulates dexamethasone-induced tetranectin gene expression during the in vitro mineralization of the human osteoblastic cell line SV-HFO, *FEBS Lett. 373*, 1−4.

9. Wewer, U. M., Ibaraki, K., Schjørring, P., Durkin, M. E., Young, M. F., and Albrechtsen, R. (1994) A potential role for tetranectin in mineralization during osteogenesis, *J. Cell Biol. 127*, 1767−1775.
10. Iba, K., Durkin, M. E., Johnsen, L., Hunziker, E., Damgaard-Pedersen, K., Zhang, H., Engvall, E., Albrechtsen, R., and Wewer, U. M. (2001) Mice with a targeted deletion of the tetranectin gene exhibit a spinal deformity, *Mol. Cell. Biol. 21*, 7817−7825.
11. Holtet, T. L., Graversen, J. H., Clemmensen, I., Thøgersen, H. C., and Etzerodt, M. (1997) Tetranectin, a trimeric plasminogen-binding C-type lectin, *Protein Sci. 6*, 1511−1515.
12. Lorentsen, R. H., Graversen, J. H., Caterer, N. R., Thøgersen, H. C., and Etzerodt, M. (2000) The heparin-binding site in tetranectin is located in the N-terminal region and binding does not involve the carbohydrate recognition domain, *Biochem. J. 347* (Part 1), 83−87.
13. Nielsen, B. B., Kastrup, J. S., Rasmussen, H., Holtet, T. L., Graversen, J. H., Etzerodt, M., Thøgersen, H. C., and Larsen, I. K. (1997) Crystal structure of tetranectin, a trimeric plasminogen-binding protein with an α-helical coiled coil, *FEBS Lett. 412*, 388−396.
14. Nielsen, B. B., Kastrup, J. S., Rasmussen, H., Graversen, J. H., Etzerodt, M., Thøgersen, H. C., and Larsen, I. K. (2000) Crystallization and molecular-replacement solution of a truncated form of human recombinant tetranectin, *Acta Crystallogr., Sect. D 56*, 637−639.
15. Graversen, J. H., Lorentsen, R. H., Jacobsen, C., Moestrup, S. K., Sigurskjold, B. W., Thøgersen, H. C., and Etzerodt, M. (1998) The plasminogen binding site of the C-type lectin tetranectin is located in the carbohydrate recognition domain, and binding is sensitive to both calcium and lysine, *J. Biol. Chem. 273*, 29241−29246.
16. Graversen, J. H., Sigurskjold, B. W., Thøgersen, H. C., and Etzerodt, M. (2000) Tetranectin-binding site on plasminogen kringle 4 involves the lysine-binding pocket and at least one additional amino acid residue, *Biochemistry 39*, 7414−7419.
17. Kluft, C., Jie, A. F., Los, P., de Wit, E., and Havekes, L. (1989) Functional analogy between lipoprotein(a) and plasminogen in the binding to the kringle 4 binding protein, tetranectin, *Biochem. Biophys. Res. Commun. 161*, 427−433.
18. Caterer, N. R., Graversen, J. H., Jacobsen, C., Moestrup, S. K., Sigurskjold, B. W., Etzerodt, M., and Thøgersen, H. C. (2002) Specificity determinants in the interaction of apolipoprotein(a) kringles with tetranectin and LDL, *Biol. Chem. 383*, 1743−1750.
19. Westergaard, U. B., Andersen, M. H., Heegaard, C. W., Fedosov, S. N., and Petersen, T. E. (2003) Tetranectin binds hepatocyte growth factor and tissue-type plasminogen activator, *Eur. J. Biochem. 270*, 1850−1854.
20. Drickamer, K. (1999) C-type lectin-like domains, *Curr. Opin. Struct. Biol. 9*, 585−590.
21. Kastrup, J. S., Nielsen, B. B., Rasmussen, H., Holtet, T. L., Graversen, J. H., Etzerodt, M., Thøgersen, H. C., and Larsen, I. K. (1998) Structure of the C-type lectin carbohydrate recognition domain of human tetranectin, *Acta Crystallogr., Sect. D 54*, 757−766.
22. Delaglio, F., Grzesiek, S., Vuister, G. W., Zhu, G., Pfeifer, J., and Bax, A. (1995) NMRPipe: A multidimensional spectral processing system based on UNIX pipes, *J. Biomol. NMR 6*, 277−293.
23. Kjær, M., Andersen, K. V., and Poulsen, F. M. (1994) Automated and semiautomated analysis of homo- and heteronuclear multidimensional nuclear magnetic resonance spectra of proteins: The program Pronto, *Methods Enzymol. 239*, 288−307.
24. Zimmerman, D. E., Kulikowski, C. A., Huang, Y., Feng, W., Tashiro, M., Shimotakahara, S., Chien, C., Powers, R., and Montelione, G. T. (1997) Automated analysis of protein NMR assignments using methods from artificial intelligence, *J. Mol. Biol. 269*, 592−610.
25. Koradi, R., Billeter, M., and Wüthrich, K. (1996) MOLMOL: A program for display and analysis of macromolecular structures, *J. Mol. Graphics 14*, 51−55 and 29−32.
26. Wütrich, K. (1986) *NMR of Proteins and Nucleic Acids*, Wiley, New York.
27. Güntert, P., Mumenthaler, C., and Wüthrich, K. (1997) Torsion angle dynamics for NMR structure calculation with the new program DYANA, *J. Mol. Biol. 273*, 283−298.
28. Herrmann, T., Güntert, P., and Wüthrich, K. (2002) Protein NMR structure determination with automated NOE assignment using the new software CANDID and the torsion angle dynamics algorithm DYANA, *J. Mol. Biol. 319*, 209−227.
29. Cornilescu, G., Delaglio, F., and Bax, A. (1999) Protein backbone angle restraints from searching a database for chemical shift and sequence homology, *J. Biomol. NMR 13*, 289−302.
30. Schwieters, C. D., Kuszewski, J. J., Tjandra, N., and Marius Clore, G. (2003) The Xplor-NIH NMR molecular structure determination package, *J. Magn. Reson. 160*, 65−73.
31. Brünger, A. T., Adams, P. D., Clore, G. M., DeLano, W. L., Gros, P., Grosse-Kunstleve, R. W., Jiang, J. S., Kuszewski, J., Nilges, M., Pannu, N. S., Read, R. J., Rice, L. M., Simonson, T., and Warren, G. L. (1998) Crystallography & NMR system: A new software suite for macromolecular structure determination, *Acta Crystallogr., Sect. D 54*, 905−921.
32. Linge, J. P., Williams, M. A., Spronk, C. A., Bonvin, A. M., and Nilges, M. (2003) Refinement of protein structures in explicit solvent, *Proteins: Struct., Funct., Genet. 50*, 496−506.
33. Ng, K. K., Park-Snyder, S., and Weis, W. I. (1998) Ca^{2+}-dependent structural changes in C-type mannose-binding proteins, *Biochemistry 37*, 17965−17976.
34. Feinberg, H., Park-Snyder, S., Kolatkar, A. R., Heise, C. T., Taylor, M. E., and Weis, W. I. (2000) Structure of a C-type carbohydrate recognition domain from the macrophage mannose receptor, *J. Biol. Chem. 275*, 21539−21548.
35. Mullin, N. P., Hall, K. T., and Taylor, M. E. (1994) Characterization of ligand binding to a carbohydrate-recognition domain of the macrophage mannose receptor, *J. Biol. Chem. 269*, 28405−28413.
36. Ng, K. K., and Weis, W. I. (1998) Coupling of prolyl peptide bond isomerization and Ca2+ binding in a C-type mannose-binding protein, *Biochemistry 37*, 17977−17989.
37. Poget, S. F., Freund, S. M. V., Howard, M. J., and Bycroft, M. (2001) The ligand-binding loops in the tunicate C-type lectin TC14 are rigid, *Biochemistry 40*, 10966−10972.
38. Poget, S. F., Legge, G. B., Proctor, M. R., Butler, P. J., Bycroft, M., and Williams, R. L. (1999) The structure of a tunicate C-type lectin from *Polyandrocarpa misakiensis* complexed with D-galactose, *J. Mol. Biol. 290*, 867−879.
39. Brown, E. M., and MacLeod, R. J. (2001) Extracellular calcium sensing and extracellular calcium signaling, *Physiol. Rev. 81*, 239−297.
40. Guex, N., and Peitsch, M. C. (1997) SWISS-MODEL and the Swiss-PdbViewer: An environment for comparative protein modeling, *Electrophoresis 18*, 2714−2723.

BI049570S